

The Promise and Challenge of Phosphorus-Based Composites as Anode Materials for Potassium-Ion Batteries

Ying Wu, Hai-Bo Huang, Yuezhan Feng, Zhong-Shuai Wu,* and Yan Yu*

Dedicated to the 70th anniversary of Dalian Institute of Chemical Physics, CAS

Potassium-ion batteries (KIBs) are a core energy storage device that can meet the need for scalable and affordable stationary applications because they use low-cost and earth-abundant potassium. In addition, KIB shares a similar storage mechanism with current Li-ion batteries. As the key to optimizing a battery's performance, the development of high-performance electrode materials helps to increase the feasibility of KIB technology. In this sense, phosphorus-based materials (i.e., phosphorus and metal phosphide) with high theoretical capacity and low redox potential tick all the right boxes as a material of choice. A rapid glimpse at recent studies on phosphorus-based anode materials for advanced KIBs is provided, covering the synthetic methods, reaction mechanisms, electrochemical properties, and performances. In addition, several promising strategies are highlighted to address the imminent challenges faced by phosphorus-based anode materials, hoping to cast an insightful outlook for possible future direction in this field.

1. Introduction

Rechargeable lithium-ion batteries (LIBs) are an essential catalyst to unlock new advances in sectors such as portable electronics, electrical vehicles, and grid-scale energy storage thanks to their high energy density and long cycling life.^[1] However, the uneven distribution and limited resource of lithium have redirected attention to other alternative rechargeable battery technologies,^[2] such as sodium-ion batteries (NIBs) and potassium-ion batteries (KIBs) that share a similar rocking-chair operation mechanism with LIBs (Figure 1a).^[3] In particular, KIBs is attractive because the standard redox potential of K^+/K (-2.93 V vs SHE) in aqueous electrolyte is lower than that of Na^+/Na (-2.71 V vs SHE) and even comparable to Li^+/Li (-3.04 V vs SHE), which allows

KIBs to sustain higher cell voltages.^[4] In addition, in the non-aqueous electrolytes, such as the propylene carbonate solvent, the standard redox potential of K^+/K (-2.88 V vs SHE) is even lower than the Na^+/Na (-2.56 V vs SHE) and Li^+/Li (-2.79 V vs SHE).^[5] Besides, weaker Lewis acidity of K^+ results in smaller solvated ions, which gives rise to higher ionic conductivity than that of Li^+ or Na^+ and translates into rapid ion diffusion kinetics.^[6] Moreover, the success of graphite in LIBs has been duplicated for KIBs. In contrast to SIBs, the intercalation of K^+ into graphite is kinetically favorable and highly reversible.^[3c,7] All the characteristics mentioned above bode well for the development of KIBs as a promising battery system that can reach parity with LIBs.

Although KIBs hold tremendous potential, there are obstacles to advancing the technology including issues related to the instability of materials upon insertion/extraction of large K^+ , leading to poor cyclability and low initial Coulombic efficiency (ICE). Ever since the breakthrough achieved by the pioneering work on graphite,^[4b] researchers have been trying to find the next leap forward by systematically interrogating suitable anode materials that feature higher specific capacity, better long-term cycling stability, and excellent rate performance. Up to now, a wide range of intercalation-type (e.g., graphite,^[3c,d,8] hard carbon,^[4a,9] heteroatoms-doped carbon,^[10] $K_2Ti_4O_9$,^[11] MoS_2 ,^[12] and MXene-derived potassium titanate^[13]), conversion-type anode materials (e.g., CoS ,^[14] and SnS_2 ^[15]), and alloying-type anode materials (e.g., Sn ,^[16] Sb ,^[17] Bi ,^[18] and P ^[5a,19]) are


Dr. Y. Wu, Prof. Y. Yu
Hefei National Laboratory for Physical Sciences at the Microscale
Department of Materials Science and Engineering
Key Laboratory of Materials for Energy Conversion
Chinese Academy of Sciences
University of Science and Technology of China
Hefei, Anhui 230026, China
E-mail: yanyumse@ustc.edu.cn

Dr. H.-B. Huang, Prof. Z.-S. Wu
Dalian National Laboratory for Clean Energy
Dalian Institute of Chemical Physics
Chinese Academy of Sciences
457 Zhongshan Road, Dalian 116023, China
E-mail: wuzs@dicp.ac.cn

Dr. Y. Feng
Key Laboratory of Materials Processing and Mold (Zhengzhou University)
Ministry of Education
Zhengzhou University
Zhengzhou 450002, China

Prof. Y. Yu
State Key Laboratory of Fire Science
University of Science and Technology of China
Hefei, Anhui 230026, China

Prof. Y. Yu
Dalian National Laboratory for Clean Energy (DNL)
Chinese Academy of Sciences (CAS)
Dalian 116023, China

 The ORCID identification number(s) for the author(s) of this article can be found under <https://doi.org/10.1002/adma.201901414>.

DOI: 10.1002/adma.201901414

investigated for KIBs. However, most of the intercalation- and conversion-type anodes fail to deliver capacity exceeding 300 mAh g^{-1} and operate at relatively high working potential of above 1.0 V (i.e., low working potential for full-cell configuration). Among them, phosphorus (P), especially black P and red P, is one of the alloying-type anode materials that stands out from the rest based on their high capacity (Figure 1b) and low redox potential.^[20] Unfortunately, the poor electronic conductivity and huge volume change during the charge/discharge processes severely limit its electrochemical performance and widespread application.^[21] The similarity in alloying reaction mechanism between different monovalent alkali metal-ion batteries enables the electrode design and modification strategies of P-based anode materials employed in LIBs and NIBs to be transposed for KIBs. Therefore, engineering P into nanodimension and combining P with conductive carbon matrix could be the solution to accommodating the volume expansion, shortening ion diffusion length, and facilitating charge transfer.^[22] For example, phosphorene, a single or few layer material delaminated from the bulk black P, exhibits intriguing properties.^[23] In addition, the incorporation of metal phases into P that leads to the formation of metal phosphides can effectively enhance the electronic conductivity and buffer the huge volume change as well as deliver higher theoretical capacity based on the dual conversion-alloying mechanism.^[24] It is worth noting that the electrolyte composition, additives as well as the binders also have great influence on the potassium storage capability of P-based anode materials. Therefore, it is of great significance to optimize the structural and surface properties of the P-based anode materials to allow the best matching electrode and electrolyte combinations to be achieved.

In this progress report, we describe key advances of P-based anode materials for KIBs (Figure 2) with a primary emphasis on the structural properties, synthesis strategies, and potassium storage mechanisms. In addition, we also summarize the current modification strategies used to improve the potassium storage performance of P-based anodes. Finally, we also share our insights on the existing challenges and opportunities for designing high-performance P-based anodes for KIBs.

2. P Anodes for KIBs

Among the alloying-typed anode materials, red P and black P are very attractive due to their ultrahigh theoretical capacity of 2596 mAh g^{-1} for LIBs and NIBs based on a three-electron alloying mechanism.^[21b] Thus, it is of great significance to explore the application potential of P anodes in KIBs. In this section, the potassium storage mechanism, the design and modification strategies of P anodes will be systematically summarized and illustrated.

2.1. Potassium Storage Mechanisms of P Anodes

Similar with the reaction toward Li and Na, P anode reacts with K through an alloying process. However, existence of rich polymorphs of potassium phosphides (e.g., K_3P , KP, K_4P_3 , K_3P_{11})^[25] poses great challenge to identify the accurate potassiation



Ying Wu currently works as a postdoctoral researcher at the University of Science and Technology of China (USTC). She received her Ph.D. in material science at USTC in 2019 under the supervision of Prof. Yan Yu. Her research interests mainly focus on the synthesis and characterization of electrode materials for Li-ion, Na-ion, and K-ion batteries.



Zhong-Shuai Wu received his Ph.D. in materials science from the Institute of Metal Research, CAS in 2011, and worked as a postdoc at the Max-Planck Institute for Polymer Research, Mainz, Germany, in 2011–2015. He then joined DICP as a full professor and group leader of 2D Materials & Energy Devices. His research focuses

on graphene and 2D materials, supercapacitors, micro-supercapacitors, batteries (Li-S/metal, Li-, Na-, K-, Zn-, Al-ion), microbatteries, flexible and planar energy-storage devices.



Yan Yu is a professor of material science at the University of Science and Technology of China (USTC). She received her Ph.D. in material science at USTC in 2006. From 2007 to 2008, she worked as a postdoctoral researcher at Florida International University. She worked at the Max Planck Institute for Solid-State Research in Stuttgart,

Germany. Her current research interests mainly include the design of novel nanomaterials for clean energy, especially for batteries and the fundamental science of energy-storage systems.

products and the potassium storage mechanism of P remains unclear. As compared to the extensive studies carried out for P anode in LIBs and NIBs, so far only limited work has been reported for P anode in KIBs. The potassium storage capability of the P-based anode materials has been first attempted by

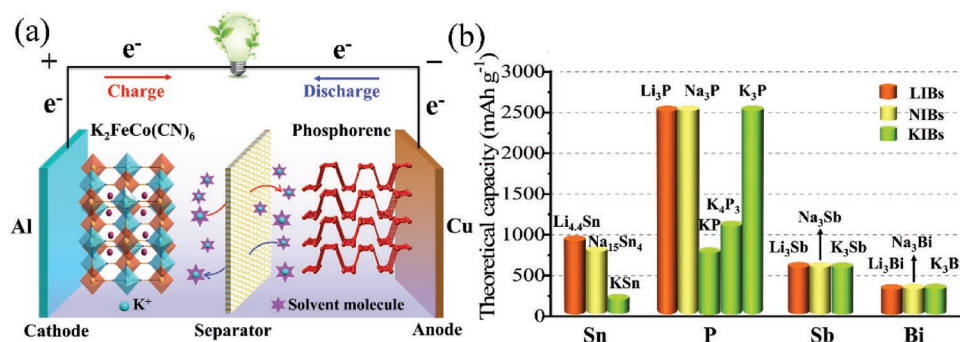


Figure 1. a) Schematic illustration of a “rocking-chair” potassium ion battery. b) The alloying mechanism and theoretical capacity of the alloying-typed anode materials for alkali cells.

Zhang et al. in 2017.^[19] They first studied the potassium storage behavior of the phosphorus-carbon (P/C) composite anode prepared by ball-milling of red P and carbon black with irregular agglomerated structure with the particles size of several micrometers. When tested in 0.8 M potassium hexafluorophosphate (KPF_6) in an ethylene carbonate (EC)/diethyl carbonate (DEC) solution ($V_{EC}/V_{DEC} = 1:1$), a high initial discharge capacity of 2171.7 mAh g⁻¹ at the current density of 50 mA g⁻¹ was achieved and the reversible capacity could be maintained at about 500 mAh g⁻¹ in the initial 3 cycles (the specific capacities and various current densities are all based on the total mass of the composite in this progress report). However, the P/C anode demonstrated fast capacity decay with the capacity dropped to zero within 30 cycles. The final potassiation product of $K_{3-x}P$ phase were detected via the ex situ X-ray diffraction (XRD), demonstrating the reversible three-electron mechanism of the P/C anode (i.e., $P \leftrightarrow K_{3-x}P$) and indicating that the P/C anode had the ability to store K^+ reversibly. In addition, Kim et al. have

computed and compared the energetics of alloying K and Na with P by the first-principles calculations based on density functional theory (DFT).^[20] As revealed in their results as shown in Figure 3a, KP and K_4P_3 are the most stable configurations of the alloying products, corresponding to a theoretical capacity of 865 and 1154 mAh g⁻¹, respectively. The alloying voltage of K_4P_3 is lower than that of KP, which might lead to higher energy density of the corresponding KIBs system. On the other hand, because of the larger size of the K ions, larger volume expansion and more drastic capacity fading is expected during the uptake and extract of K ions (Figure 3b). These theoretical predictions have been partly confirmed by the later experimental reports. For example, Sultana et al.^[5a] fabricated the black phosphorus-graphite (BP-C) composite via ball-milling as anode material for KIBs. When cycled in a 0.75 M KPF_6 /EC/DEC ($V_{EC}/V_{DEC} = 1:1$) electrolyte, the higher specific capacity of >600 mAh g⁻¹ could be achieved in the BP-C anode with a mass ratio of $m_{BP}:m_C = 7:3$ (BP-C 7:3). What is more, in order to explore the alloying mechanism, ex situ XRD pattern was conducted. After the first discharge to 0.01 V versus K/K⁺, a series of peaks corresponding to KP phase appeared. The XRD result indicates a new alloying process with the formation of KP phase after complete potassiation, which is different from the three-electron reaction mechanism in Zhang's study.^[19] Based on the detected KP-type alloy phase, the authors further proposed a possible reaction mechanism: $P + K^+ + e^- \rightleftharpoons KP$, demonstrating a theoretical capacity of 865 mAh g⁻¹. In the next study, Xiong et al.^[22] studied the potassium storage performance of the P anode with tiny red P particles (10–20 nm) embedded into 3D interconnected porous carbon nanosheets (red P@CN composite) via the vaporization-condensation strategy. The electrical conductivity of the products is increased, confirming the successful alloying of K with P. At the same time, the thickness of electrode increased from 14.9 to 16.9 μm. The reversible cathodic and anodic peaks at ≈0.16 and ≈0.72 V were assigned to the potassiation and depotassiation process of red P, which is corresponding to the slope shape centered at ≈0.25 V and a voltage plateau at ≈0.72 V in the charge/discharge voltage profiles (Figure 3c,d). The ex situ high-resolution transmission electron microscopy (HRTEM) and selected area electron diffraction (SAED) pattern (Figure 3e) detected a nanocrystallite structure of KP phase at the fully discharged state, which was further confirmed by ex situ XRD measurements (Figure 3f). Therefore, they proposed that the final potassiation product of

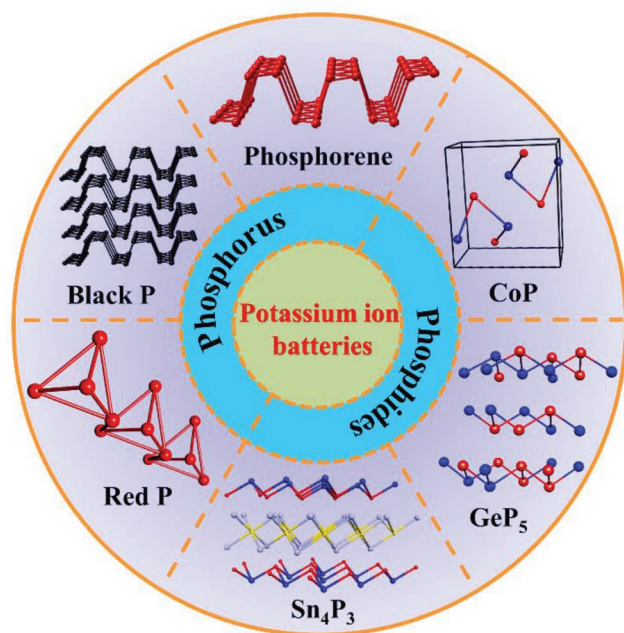


Figure 2. Schematic illustration of the phosphorus-based composites as anode materials for KIBs.

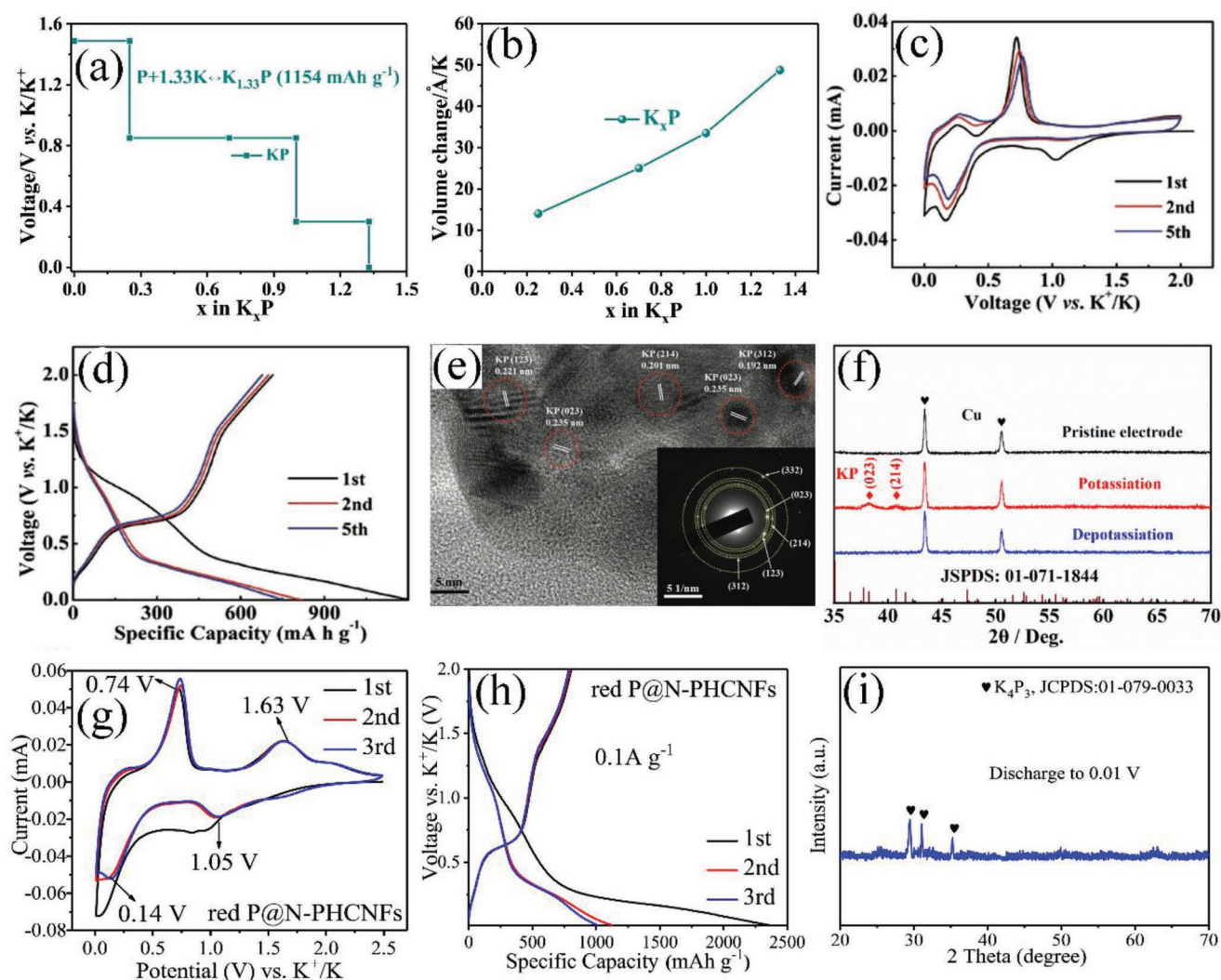


Figure 3. a) Voltage–composition curves calculated for potassium alloying; b) Volume expansion upon potassium phosphorus compounds as a function of x in K_xP . Reproduced with permission.^[20] Copyright 2018, Wiley-VCH. c,d) CV curves and galvanostatic discharge–charge profiles of red P@CN composite; e) HRTEM image and SAED patterns of red P@CN electrodes: potassiation state at 0 V; f) Ex-situ XRD patterns of the red P@CN anode. Reproduced with permission.^[22] Copyright 2018, Wiley-VCH. g,h) CV curves and galvanostatic discharge–charge profiles for the initial three cycles at 0.1 A g^{-1} of the red P@N-PHCNFs anode; i) Ex-situ XRD pattern of the red P@N-PHCNFs-5. Reproduced with permission.^[26] Copyright 2019, American Chemical Society.

red P@CN anode was KP, via the reaction of $P + K^+ + e^- \rightleftharpoons KP$, leading to a theoretical capacity of 865 mAh g^{-1} . In the latest study,^[26] our group designed and fabricated a unique free-standing nitrogen-doped porous hollow carbon nanofibers as the matrix for the encapsulation of red P (red P@N-PHCNFs) via the vaporization-condensation approach. Two reversible peaks located at 1.05 and 0.14 V were displayed, corresponding to the stepwise potassiation of red P in the discharge process. In the charging step, two peaks located at 0.74 and 1.63 V revealed the stepwise depotassiation process (Figure 3g). This cyclic voltammetry (CV) behavior is well consistent with the voltage–composition curves calculated by Kim et al.^[20] In addition, the plateaus and slopes in the charge/discharge profiles were well consistent with the redox behavior in the CV scans, which further confirmed the accuracy of the electrochemical data (Figure 3h). Ex situ XRD test was also performed with

detection of the potassiation product as K_4P_3 (Figure 3i). Thus, the reaction mechanism of red P@N-PHCNFs was proposed as: $3P + 4K^+ + 4e^- \rightleftharpoons K_4P_3$, corresponding to a theoretical capacity of 1154 mAh g^{-1} . It is possible that the morphology structure (e.g., particles size), hybridization (e.g., carbonaceous matrix), or the electrochemical window have great influence on the depth of discharge of P anode in KIBs, which leads to distinctive interpretation of the reaction mechanism. It would be of great significance to develop advanced in situ characterizations such as in situ XRD, Raman, and TEM to directly and precisely evaluate the detailed potassiation/depotassiation processes.

2.2. Challenges toward P Anodes

Despite great progress has been made in the development of P anodes for KIBs, they still face the following challenges:

- 1) Poor electronic conductivity: The intrinsically low electronic conductivity of red P (10^{-14} S cm $^{-1}$) has limited its K $^{+}$ diffusion kinetics and utilization of active materials, which leads to large electrochemical polarization and fast capacity decay.^[26]
- 2) Volume expansion: Large volume change during the repeated potassiation/depotassiation processes based on the alloying reaction leads to pulverization of the P anodes and loss of electrical contact with the current collector, resulting in severe capacity decay and rapid cell failure.^[27]
- 3) Unstable solid electrolyte interface (SEI): The gradual pulverization of P anodes caused by large volume change tend to destroy the SEI layer and the fresh naked surface of P anodes prone to continuous SEI growth by consuming excess K $^{+}$ and electrolyte, resulting in the capacity decay and low Coulomb efficiency.^[28]

2.3. Modification Strategies for P Anodes

In order to overcome the bottleneck of P anodes for KIBs mentioned above, researchers are looking into ways to optimize the performance through materials modification and engineering. Strategies in recent studies mainly focus on design of nanostructured P anodes, hybridization of P, and conductive buffering matrix as well as optimization of the electrolyte composition.

2.3.1. Hybridization of P and Carbon Materials

Hybridization of P and carbon-based materials has been proved to be an effective strategy by harnessing the benefits arises from the conductive matrix: 1) enhance the electronic conductivity of P anodes by forming P/C composite and promote fast charge transfer between the carbon network and P component; 2) shorten the K $^{+}$ diffusion length by enhancing the contact area between the P anodes and the electrolyte through the high surface area and abundant pores of carbon matrix; 3) enhance the structural stability and generate stable SEI layer by accommodating huge volume change of P anodes, improving the cycle stability of the P/C composite anodes.^[29]

As mentioned above, Sultana et al.^[5a] fabricated the BP-C composite via ball-milling as anode material for KIBs. As shown in Figure 4a, the secondary aggregated P/C particles prepared by mixing of P and carbon component displayed a wide size distribution ranging from hundreds of nanometers to tens of micrometers. As shown in Figure 4b, the BP-C anode with a mass ratio of $m_{BP}:m_C = 1:1$ (BP-C 1:1) delivered a high capacity of 443 mAh g $^{-1}$ and maintained at 270 mAh g $^{-1}$ after 50 cycles at 50 mA g $^{-1}$, corresponding to 61% capacity retention. Besides, the BP-C 1:1 also exhibited enhanced rate capability, where a specific capacity of 120 mAh g $^{-1}$ is sustained at a high current density of 50 mA g $^{-1}$ (Figure 4c). Following this success, Chang et al.^[30] further developed a ball-milling process to obtain well-mixed RP/C composite that is made up of red P particles in ketjen black (KB) and multiwalled carbon nanotube (MWCNT) (Figure 4d). When cycled in 1 M potassium bis(tri fluoromethanesulfonyl)imide (KTFSI) + EC/DEC

($V_{EC}/V_{DEC} = 1:1$) electrolyte, the RP/C delivered a reversible capacity of about 200 mAh g $^{-1}$ at 1000 mA g $^{-1}$ and showed almost no capacity decay after 60 cycles (Figure 4e). In this study, although the red P showed large particle sizes ranging from 200 to 500 nm, the red P fully covered with MWCNT and KB could effectively enhance the electric conductivity and structure strength, leading to superior long-term cycling performance. In addition, the introduction of P–C or P–O–C chemical bonds has been widely studied and confirmed to be an effective strategy to enhance the electrical contact between P and carbon matrix and enhanced the structural stability of the P/C composite.^[31] For example, Wu et al.^[32] synthesized black phosphorus/carbon composite (P/C) with abundant P–C and P–O–C chemical bonds through ball-milling, as shown in Figure 4f. Apart from the formation of the fine P/C particles (about 50 nm), the P–C and P–O–C chemical bonds are responsible for the excellent electrochemical performances. When tested in 0.8 M KPF $_6$ + EC/DEC ($V_{EC}/V_{DEC} = 1:1$) electrolyte, as shown in Figure 4g, the ball-milled P/C composite delivered an initial charge capacity of 482.9 mAh g $^{-1}$ at 50 mA g $^{-1}$ and 323.5 mAh g $^{-1}$ was remained after 50 cycles, corresponding to 67% capacity retention. In addition, the CV curves at different scan rates indicated the much enhanced K $^{+}$ diffusion coefficient of the P/C anode, as shown in Figure 4h. In this study, the enhanced cycling stability was ascribed to the small P/C particle size as well as the formation of stable P–C bonds that helps to ameliorate the volume expansion of P.

Despite previous studies have demonstrated the viability of ball-milling method to fabricate the P/C composites with small primary particles, intimate contact between conductive carbon matrix and P as well as abundant P–C or P–O–C chemical bonds, this method still fails to further reduce the particle size of P to nanoscale level. This eventually leads to degradation in performance arises from poor electrical contact between current collector and active materials and limited coverage of carbon to effectively accommodate the huge volume change of P anodes. Therefore, it has to be coupled with other synthetic strategies in order to boost the electrochemical performances of P anodes to a higher level.

2.3.2. Nanostructures

Nanostructuring can endow P anodes with enhanced reactivity and electronic conductivity arises from the quantum confinement effect. In addition, nanosized P particles with high specific surface can facilitate ion and electron transfer. More importantly, P nanoparticles can greatly alleviate mechanical stress caused by volume change during the potassiation/depotassiation processes, which effectively improves the long-term cycling stability.^[29]

In recent studies, the vaporization-condensation strategy has been widely employed to prepare ultrafine red P particles as well as hybridization of P and porous carbon matrix. For example, as mentioned in Xiong et al.'s study,^[22] the red P@CN composite (the size of red P particles ranges from 10 to 20 nm) was produced by this strategy. When applied as the anode for KIBs, the red P@CN composite delivered an initial charge capacity of 404.5 mAh g $^{-1}$ at 100 mA g $^{-1}$, with a capacity

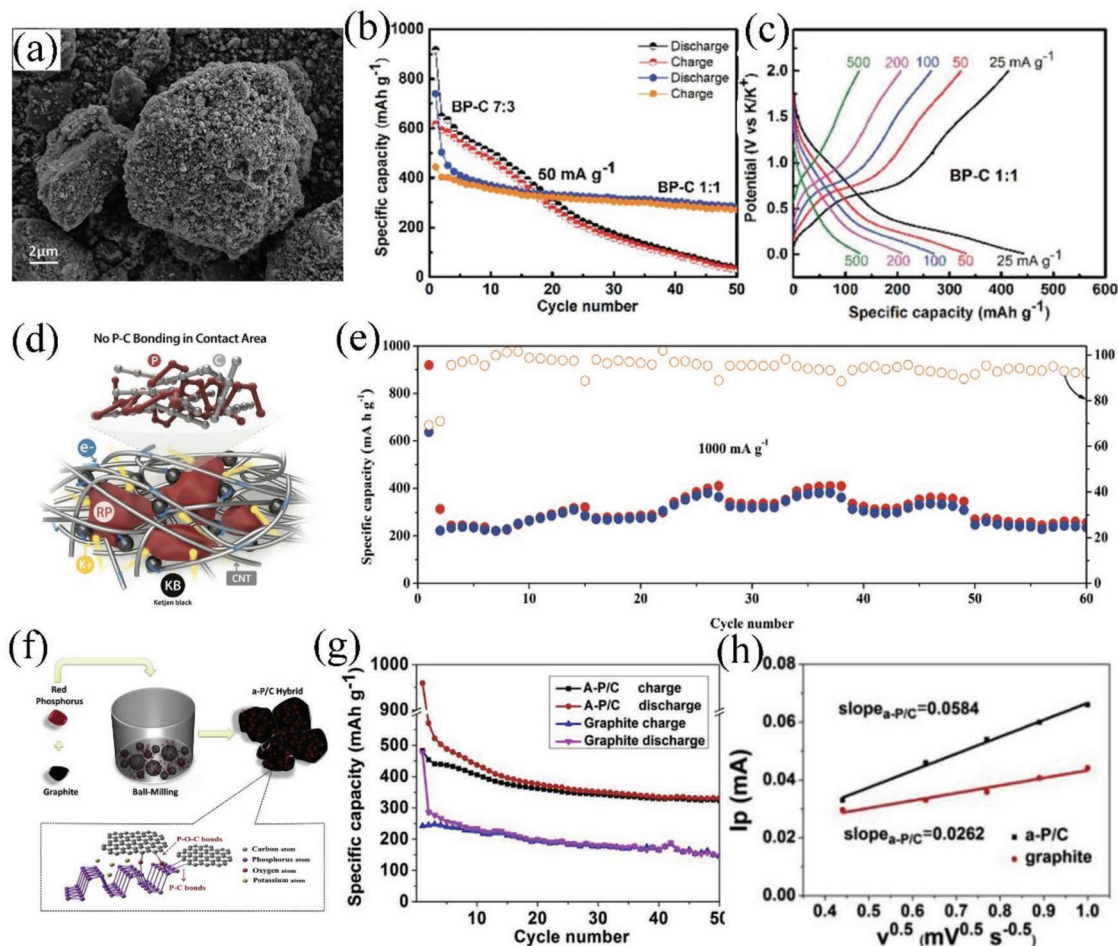


Figure 4. a) SEM image of the BP-C composite; b) Cycling performance of the BP-C anode at 50 mA g⁻¹; c) rate capability of the BP-C 1:1 anode. Reproduced with permission.^[5a] Copyright 2017, Royal Society of Chemistry. d) Schematic illustration of structural configuration of the RP/C anode; e) The cycling performance of RP/C anode at 1000 mA g⁻¹. Reproduced with permission.^[30] Copyright 2019, Wiley-VCH. f) Schematic diagram of the synthesis of the P/C composite; g) The cycling stability of the P/C anode at 50 mA g⁻¹; h) Peak current versus *v*^{0.5} and the corresponding linear fits. Reproduced with permission.^[32] Copyright 2018, Elsevier.

retention of 64% after 40 cycles. The capacity decay possibly arises from incomplete carbon coating. Therefore, full embedding of P into carbon matrix is very crucial. Inspired by this, Liu et al.^[33] further synthesized a carbon nanotube-backed mesoporous carbon for the impregnation of red P via the vaporization-condensation approach (red P@TBM composite). Red P was completely encapsulated into the mesoporous carbon, and the porous structure was well maintained after phosphorization. When cycled in 0.6 M KPF₆ + EC/PC (*V*_{EC}/*V*_{PC} = 1:1) electrolyte at 0.05 A g⁻¹, the red P@TBM anode delivered an initial charge capacity of 490.9 mAh g⁻¹ with a high capacity retention of 83% after 75 cycles. The red P@TBM anode even demonstrated excellent rate capability, delivering a specific capacity of 136 mAh g⁻¹ at the high current density of 2 A g⁻¹. In this unique structure, the MWCNTs core could effectively facilitate the electron transfer while the carbon layer with abundant mesopores could load appropriate amounts of P and provide buffering space to accommodate the huge volume change during the potassiation/depotassiation processes. In addition, the above-mentioned Wu et al.'s study showed that,

with the encapsulation of red P, the hollow fibrous structure could be well maintained without severe aggregation or pulverization, indicating that the ultrafine red P nanoparticles well embedded into the micropores of the conductive carbon matrix. The unique free-standing red P@N-PHCNFs anode demonstrated unprecedented long cycle life in addition to its ultrahigh reversible capacity,^[26] e.g., delivering high reversible capacity of 465 and 282 mAh g⁻¹ at high current density of 2 and 5 A g⁻¹ even after the long cycling of 800 cycles respectively. On top of that, volume expansion as small as 26% without any unstable structural changes such as cracking and fracture was observed under in situ TEM when potassiation process occurs on a single red P@N-PHCNF. The unprecedented potassium storage performance could be ascribed to the homogeneous encapsulation of tiny red P particles within the unique carbon matrix that resulted in faster charge transfer and K⁺ diffusion coefficient.

Based on the above-mentioned results, vaporization-condensation method is capable of synthesizing red P particles in nanoscale and homogeneously confines red P into the pores and inner surface of the carbon matrix. The confinement effect

Table 1. Comparison of the synthetic methods, structural properties, electrolyte, discharge products, and electrochemical performance of the P/C composite anodes in KIBs. (Vaporization-condensation is denoted as V-C; the carbon content of “≈x%” represents the carbon content based on the “raw material ratio”).

Anode	Synthetic methods	Structural properties	Discharge products	Test methods	Electrolyte	Carbon content [wt%]	ICE	Potassium storage performance (based on P/C composite)	Ref.
BP-C	Ball-milling	Hundreds of nanometers to tens of micrometers	KP	Ex situ XRD	0.75 M KPF ₆ in EC/DEC	≈50%	60%	443 mAh g ⁻¹ with 61% retention after 50 cycles at 50 mA g ⁻¹	[5a]
RP/C composite	Ball-milling	Red P particles of 200–500 nm covered with MWCNT and KB	KP	Ex situ XRD	1 M KTFSI in EC/DEC	≈64%	68.3%	200 mAh g ⁻¹ at 1000 mA g ⁻¹ and could cycle as long as 60 cycles without capacity decay	[30]
Black P/C composite	Ball-milling	P/C aggregated particles of about 50 nm; P–C or P–O–C chemical bonds	KP	Ex situ XRD	0.8 M KPF ₆ in EC/DEC	84%	50.3%	482.9 mAh g ⁻¹ with 67% retention after 50 cycles at 50 mA g ⁻¹	[32]
Red P@CN	V-C	Red P particles of 10–20 nm in 3D interconnected porous carbon nanosheets	KP	HRTEM; SAED Ex situ XRD	0.8 M KPF ₆ in EC/DEC	36%	59%	404.5 mAh g ⁻¹ with 64% retention after 40 cycles at 100 mA g ⁻¹	[22]
Red P@TBMC	V-C	Ultrafine red P in the 3D mesoporous carbon	KP	—	0.6 M KPF ₆ in EC/PC	60%	63.5%	490.9 mAh g ⁻¹ with 83% retention after 75 cycles at 50 mA g ⁻¹	[33]
Red P@N-PHCNFs	V-C	Ultrafine red P in the nitrogen-doped porous hollow carbon nanofibers	K ₄ P ₃	CV Ex situ XRD In situ Raman	0.7 M KPF ₆ in EC/DEC	34%	—	795 mAh g ⁻¹ with 82% retention after 100 cycles at 100 mA g ⁻¹	[26]

allows the stress caused by volume change to be effectively alleviated without affecting the morphology and microstructure of the carbon matrixes, thus improving the long-term cycling performance. For example, Wu et al.^[26] claimed that the 3D linked hollow carbon nanofibers synthesized via vaporization-condensation method could promote the penetration of electrolyte, thus facilitating the diffusion of K⁺. The fibrous structure with high aspect ratio and good electronic conductivity can effectively promote the rapid electron transfer of electrons in the radial direction and shorten the diffusion distance of K⁺ in the vertical fiber direction. The abundant micropores in the carbon matrix can serve as the storing space for red P and reduce the absolute strain and preventing pulverization and agglomeration, as well as the hollow cavity could buffer the volume change, guaranteeing the good structural stability. The formed P–C chemical bonds during vaporization-condensation process and the N-doping in the carbon nanofiber with much higher adsorption energy could facilitate the electrical contact and protect the structural stability. Based on the above-mentioned synergistic effect, the red P@N-PHCNFs anode demonstrates the unprecedented potassium storage performance. In addition, for the selection of a suitable carbon matrix for red P loading via the vaporization-condensation method, Yao et al.^[31d] used the molecular dynamics simulations and density functional theory calculations for screening of carbon matrix with desired pore properties, who proposed that micropores ranging from 1 to 2 nm in diameter and the formation of P–O–C chemical bonding are essential for realizing high P loading and giving rise to a stable composite structure. In addition to the vaporization-condensation method, the vapor-redistribution strategy

could also effectively downsize the red P particles with uniform distribution in the carbon matrix as studied in NIBs system.^[34]

In addition to the design of nanosized P, just like NIBs system, engineering P anodes with hollow cavity is another effective strategy to accommodate huge volume change during the charge/discharge process, resulting in better long-term cycling stability. For example, Zhou et al.^[35] employed a solvothermal method to fabricate the hollow porous pure red P nanospheres (HPNs-300) via a gas-bubble-directed formation mechanism. High specific capacity of 1048.4 mAh g⁻¹ at 1 C could be maintained at 1 C even after 600 cycles almost without significant capacity decay. In addition, in recent researches in NIBs, Liu et al.^[36] further developed the reduction of phosphorus halide precursor (PI₃) method combining with the gas-bubble-directed formation to fabricate the porous red P spheres on graphene (NPRP@RGO). The outstanding long cycling performance could be achieved as long as 1500 cycles almost no capacity decay. For the two unique red P anodes, the outstanding long cycling performance could be attributed to the hollow porous P structure, which has free space to accommodate the huge volume change and thus avoid pulverization.^[36,37]

To provide an overview of the current status of P anodes, their synthetic methods, structural properties, electrolyte composition, potassium storage mechanism, and electrochemical performance of P anodes KIBs are summarized in **Table 1**. In short, there are some criteria for achieving enhanced potassium storage capability, which are smaller particle size, intimately link with conductive carbon network, encapsulation of ultrafine P into the microporous carbon matrix, formation of P–C/P–O–C chemical bonds.

2.3.3. Optimization of Electrolytes and Binders

Electrolyte compositions, such as potassium salts, solvents as well as additives, have great influence on the performance of P anodes in KIBs. Optimization of the electrolyte composition leads to the formation of uniform and stable SEI layer and reduces side reactions, which is a critical parameter in determining the potassium storage performance. For example, inspired by the positive effects of fluoroethylene carbonate (FEC) during the formation of stable SEI layer in NIBs system,^[38] Chang et al. attempted to duplicate its success to KIBs by evaluating the RP/C anode in the electrolyte containing FEC. However, the capacity was limited to only 3 mAh g⁻¹ at 100 mA g⁻¹, indicating that FEC is not an effective as additive for RP/C in KIBs.^[39] In addition, the binders also have great influence on the electrochemical performance of P anodes, especially ICE. Wu's study showed that sodium carboxymethyl cellulose (CMC-Na) binder without defluorination effect could effectively improve the ICE, capacity and cycling stability of P/C anodes.^[32] Overall, up to now, the research on the electrolytes and binders for the P anodes in KIBs are still very limited. Therefore, it is of significance to investigate their influence on P anodes in order to achieve enhanced potassium storage capability.

3. Metal Phosphide Anodes for KIBs

The poor intrinsic electronic conductivity of P as well as the large strain induced by the volumetric expansion severely limits the improvement of the potassium storage performance of P anodes. To overcome these problems, apart from rational design of nanostructures and hybridizing with conductive matrix, transforming the elemental P into metal phosphides, such as FeP, CoP, GeP₅, SnP₃, and so forth, could be an alternative way to enhance the potassium storage performance.^[40] The metal phosphides exhibit the metallic features and excellent thermal stability. During the discharge process, the nano-sized metallic nanocrystals formed through the conversion reactions can serve as the highly conductive electronic channels that enable fast charge transfer kinetics and an elastic matrix to buffer the huge volumetric stress arising from the potassium phosphorus compounds.^[41] In addition, when used as anode materials for KIBs, the metal phosphides can still deliver higher theoretical capacity based on the conversion-alloying mechanism compared with most of the carbonaceous anodes and conversion-type anodes. However, the huge volume change remains an unresolved issue that needs to couple with other modification strategies to overcome it in order to further improve the potassium storage properties of P anodes.

3.1. Potassium Storage Mechanism of Metal Phosphide Anodes

Metal phosphides can be classified into two categories based on the reactivity of the metal component with potassium.

- 1) Metal (inactive) phosphides: For the metal (inactive) phosphides, such as the Fe-P,^[42] Co-P,^[43] Ni-P.^[44] For the metal

(inactive) phosphides, there is no doubt that the inactive metal phase can enhance the electronic conductivity and buffer the structural stress after they are reduced to metallic phase. The capacity of the metal (inactive) phosphides is contributed merely by the P component. The potassium storage mechanism of the metal (inactive) phosphides could be summarized as follows

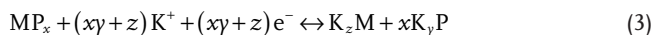


The theoretical capacity based on the formation of the final product of K_yP alloy could be calculated according to Equation (2)

$$C = \frac{xyF}{3.6M_{w(\text{MP}_x)}} \quad (2)$$

where $F = 96\,500\text{ C}$ (Coulombs), $1\text{ C} = 0.2777\text{ mAh}$.

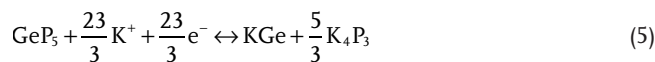
- 2) Metal (active) phosphides: For the metal (active) phosphides, such as Ge-P,^[45] Sn-P.^[41c] For the metal (active) phosphides, both elements could reversibly alloy with K⁺, which contributes to the higher theoretical capacity, but is usually accompanied by a larger volume change during potassiation/depotassiation process. The potassium storage mechanism of metal (active) phosphides could be summarized as follows



The theoretical capacity based on the formation of the final product of K_yP alloy could be calculated according to Equation (4)

$$C = \frac{(xy + z)F}{3.6M_{w(\text{MP}_x)}} \quad (4)$$

For example, Guo's group^[46] pioneered the investigation of the potassium storage mechanism of the GeP₅ anode. According to the results of the contour plots obtained from in operando synchrotron XRD ($\lambda = 0.68\,899\text{ \AA}$) shown in Figure 5a–d, the alloying/dealloying process of the GeP₅ anode is schematically illustrated in Figure 5e. During the discharge process, the conversion reaction first occurs, which leads to the formation of Ge and K₄P₃ phase. When further discharged to 0.45 V, the intensity of the Ge reflection increases to its maximum and then decreases. After further discharged to 0.04 V, the peak of the KGe reflection starts to appear and remains high until full discharge. In general, the potassiation process of GeP₅ could be divided into two stages and could be summarized in the following equations



The theoretical capacity of GeP₅ anode in KIBs in this study can be calculated to be 903 mAh g⁻¹. The high theoretical capacity based on the final potassiation products of KGe and K₄P₃ compounds shows that GeP₅ anode is a promising anode material in KIBs.

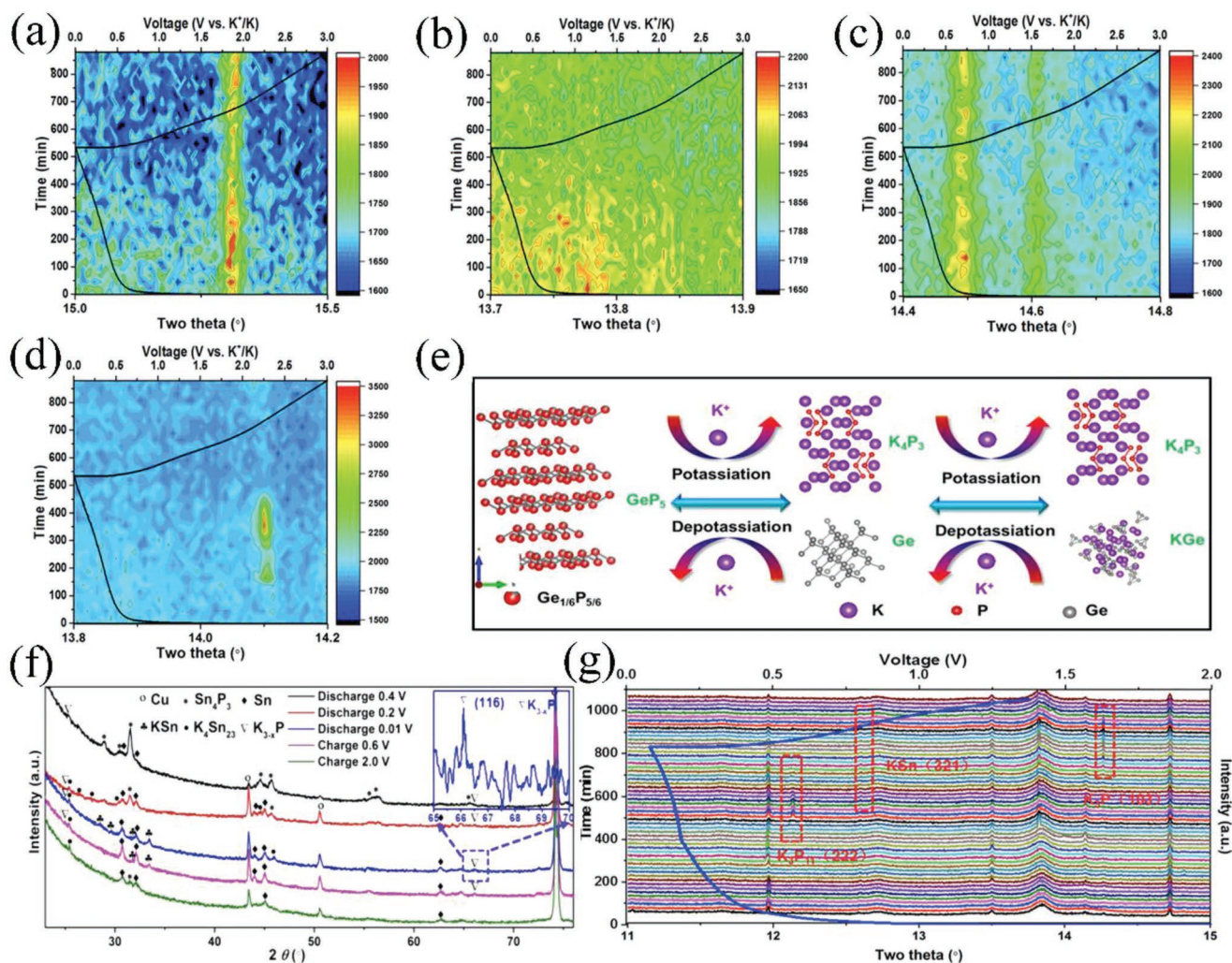
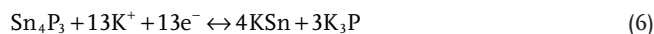


Figure 5. a–d) Contour plots of in operando synchrotron XRD with superimposed voltage profiles shown for selected 2θ ranges of GeP₅ as anode for KIBs: a) GeP₅ (012), b) K₄P₃ (114), c) Ge (201), d) KGe (215); e) Schematic illustration of the potassiation/depotassiation process in GeP₅ electrode. Reproduced with permission.^[46] Copyright 2018, Elsevier. f) Ex situ XRD patterns of cycled Sn₄P₃/C and enlarged area (65°–70°) at 0.01 V at discharged potential (inset). Reproduced with permission.^[19] Copyright 2017, American Chemical Society. g) In operando synchrotron XRD patterns of Sn₄P₃ anode for KIBs. Reproduced with permission.^[24] Copyright 2018, Elsevier.

In addition, Zhang et al.^[19] investigated the potassium storage mechanism of Sn₄P₃ anode for KIBs via ex situ XRD. As shown in Figure 5f, when first discharged to 0.4 V, the XRD signals belonging to K_{3–x}P phase emerges. When further discharged to 0.2 V, Sn phase appears and becomes the dominant phase accompanied by a diminish of the Sn₄P₃ phase. Meanwhile, several new peaks of K₄Sn₂₃ are observed. After a full discharge to 0.01 V, KSn phase could be observed. Based on the above results, the potassiation products for Sn₄P₃ anode was determined to be KSn and K_{3–x}P phases. In order to obtain the potassium storage mechanism of Sn₄P₃ anode accurately and persuasively, Zhang et al.^[24] further employed an in operando synchrotron XRD patterns (λ = 0.688 273 Å) to investigate the Sn₄P₃@carbon fiber anode for KIBs. As shown in Figure 5g, the final potassiation products of KSn and K₃P phases could be detected. The potassiation/depotassiation process could be then described by the following equations



The theoretical capacity of Sn₄P₃ anode for KIBs can be calculated to be 614 mAh g^{−1}. The in operando synchrotron XRD patterns of the Sn₄P₃@carbon fiber anode provided the researchers with a rather accurate explanation with the determination of the final potassiation products of KSn and K₃P phases. Besides, phosphorization of Sn to Sn₄P₃ could significantly enhance its theoretical capacity.

Based on the in operando synchrotron XRD results, a question arises regarding the difference in the depth of the discharge process of the P component between GeP₅ and Sn₄P₃? It is postulated that their final products differ from each other could be due to the difference in chemical bonds between Ge–P and Sn–P or the combination of different carbon matrix. Therefore, in-depth study should perform to reduce the gap in understanding the potassium storage mechanism of metal

phosphides. In this regard, elucidation of the potassiation/depotassiation process can be done through in situ techniques, such as in situ XRD, in situ Raman, and in situ TEM. Coupled them with electrochemical characterizations, such as CV, Galvanostatic intermittent titration technique (GITT), electrochemical impedance spectroscopy, the reaction mechanism of metal phosphides in KIBs can be unraveled.

3.2. CoP Anode

CoP is a promising anode material with excellent electronic conductivity and high theoretical capacity based on the conversion-alloying mechanism for LIBs.^[43] Additionally, CoP, a kind of metal (inactive) phosphide, possesses less volume expansion than the metal-(active)-type phosphides (e.g., GeP_5 and Sn_4P_3) due to little volume expansion of inactive Co metal, showing great potential for KIBs.^[47]

Bai et al.^[47] first investigated the potassium storage performance of CoP anode with core-shell-like morphology (several tens of nanometers) embedded in the N, P co-doped porous carbon sheets matrix (CoP@NPPCS, Figure 6a). When cycled in 1 M KPF_6 + EC/DMC/DEC ($V_{\text{EC}}/V_{\text{DMC}}/V_{\text{DEC}} = 1:1:1$) electrolyte, there was almost no capacity fading and reversible capacity of 127 and 114 mAh g^{-1} could be maintained at 0.1 and 0.5 A g^{-1} after 1000 cycles, respectively (Figure 6b). However, the

potassium storage mechanism of CoP was not studied in this work. Though the potassium storage mechanism of CoP was not studied in this work, their preliminary results did indicate the feasibility of CoP as anode for KIBs.

3.3. GeP_5 Anode

Germanium phosphide (GeP_5), a layered structure with the highest concentration of P element among all the binary metal phosphides, displays higher metallic conductivity than that of black P and even comparable to that of graphite.^[48] In principle, GeP_5 delivers ultrahigh volumetric capacity with fast charge transfer efficient and ion diffusion kinetics. Based on these advantages, many studies have been carried out to examine the electrochemical performance of GeP_5 anode for KIBs.

As mentioned above, Guo's group^[46] investigated the potassium storage performance of the irregular agglomerated GeP_5 microparticles that was prepared by ball-milling method (Figure 6c). The effect of the potassium salts and additives of electrolytes on the potassium storage performance of GeP_5 anode were thoroughly evaluated. This study proposed that, compared with the KPF_6 and FEC additive in electrolyte, the KFSI potassium salt in carbonate solvents could effectively facilitate the formation of uniform and thin SEI layer, as well as weaken the side reactions, thus enabling the improved

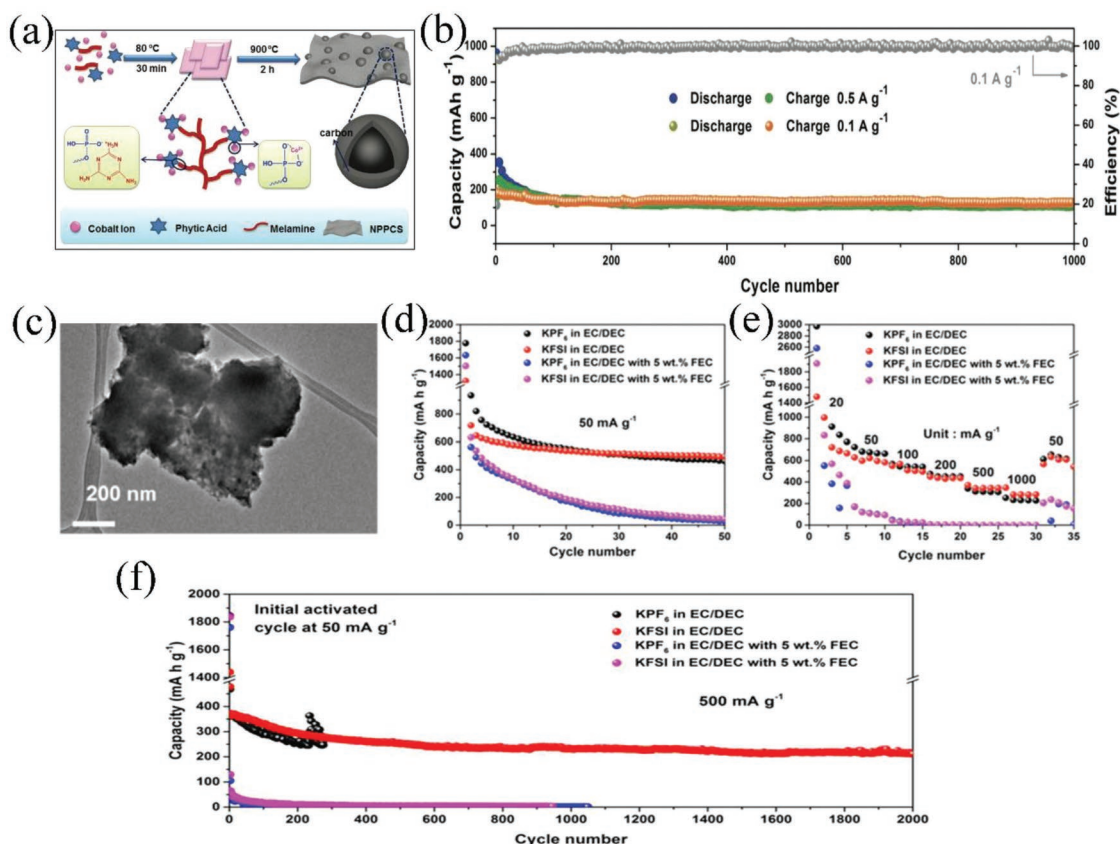


Figure 6. a,b) Schematic of the synthesis process and the cycling performance of CoP@NPPCS anode. Reproduced with permission.^[47] Copyright 2018, Wiley-VCH. c) TEM image of the GeP_5 powder; d–f) Cycling performance and rate capabilities of GeP_5 anode. Reproduced with permission.^[46] Copyright 2018, Elsevier.

CE and long cycling stability. When evaluated in 1 M KFSI + EC/DEC ($V_{EC}/V_{DEC} = 1:1$) electrolyte, the GeP_5 anode exhibited a stable cycling performance with a capacity of 495.1 mAh g^{-1} at 50 mA g^{-1} after 50 cycles (Figure 6d). As shown in Figure 6e, excellent rate capability was also achieved. Even cycled at a high current density of 500 mA g^{-1} , the GeP_5 anode also demonstrated superior cycling performance of 213.7 mAh g^{-1} capacity after 2000 cycles (Figure 6f). The nanosized metallic nanocrystals of Ge formed during the discharge process could serve as the highly conductive electronic channels that enables fast charge transfer kinetics and an elastic matrix to buffer the huge volumetric contraction of K_4P_3 . In addition, the potassiation products of K_4P_3 phase and KGe alloy can also create a mutual buffer function, which could effectively accommodate the volume changes. The high theoretical capacity with the potassiation products of KGe and K_4P_3 compounds enables GeP_5 anode a promising anode material in KIBs. High theoretical capacity can be claimed for GeP_5 if full potassiation that gives rise to the formation of KGe and K_4P_3 is achieved, which make it a very promising anode material for KIBs.

3.4. Sn_4P_3 Anode

Similar with the GeP_5 anode in KIBs, the incorporation of metallic Sn and red P component to form Sn_4P_3 could effectively increase the enhanced theoretical capacity, improve electronic conductivity as well as accommodate the huge volume change of the P component during potassiation/depotassiation process. Meanwhile, the P and the potassiation products of K-P alloy could prevent the aggregation and disperse the structural stress of the formed Sn particles during cycling. However, the volume change caused by the conversion-alloying mechanism still exists.^[29b] Therefore, design of nanostructured Sn_4P_3 as

well as the incorporation of conductive buffering matrix are still needed.

As mentioned in Zhang et al.'s study,^[19] irregular agglomerated microsized Sn_4P_3 particles were distributed in the amorphous carbon matrix. The $\text{Sn}_4\text{P}_3/\text{C}$ anode showed rapid capacity decay only after 30 cycles due to the pulverization of the aggregated particles and the formation of cracks during the continuous charge/discharge processes, leading to severe capacity decay and the failure of the cells. Afterward, they further optimized the structure of the $\text{Sn}_4\text{P}_3/\text{C}$ composite, i.e., the as-milled Sn_4P_3 nanoparticles (less than 350 nm) embedded in the N-doped carbon fibers via the electrospinning method, which could effectively buffer the large volume variations of Sn_4P_3 during cycling.^[24] When cycled at 50 mA g^{-1} in 1 M KFSI + EC/DEC electrolyte, the $\text{Sn}_4\text{P}_3/\text{C}$ carbon fiber electrode exhibited very stable cycling performance with a capacity of 403.1 mAh g^{-1} even after 200 cycles as well as the stable long-term cycling stability up to 1000 cycles (Figure 7a,b). Comparing the above two studies conducted by Zhang et al., the $\text{Sn}_4\text{P}_3/\text{C}$ fibrous structure as well as the optimization of electrolyte composition enable excellent potassium storage capability. Furthermore, Li et al.^[4c] developed a solvothermal method to successfully fabricate the $\text{Sn}_4\text{P}_3/\text{C}$ composite with Sn_4P_3 particles embedded in the hierarchically porous carbon (Figure 7c–e). When cycled in 0.8 M KPF_6 + EC/DEC ($V_{EC}/V_{DEC} = 1:1$) electrolyte, the $\text{Sn}_4\text{P}_3/\text{C}$ anode showed a high initial charge capacity of 431 mAh g^{-1} at the current density of 100 mA g^{-1} , and displayed 73% capacity retention after 100 cycles. The superior potassium storage performance of the $\text{Sn}_4\text{P}_3/\text{C}$ anode could be attributed to its unique structure: 1) the hierarchically porous carbon matrix enhances the electronic conductivity of the $\text{Sn}_4\text{P}_3/\text{C}$; 2) the hierarchically pores provide sufficient space to store Sn_4P_3 particles and accommodate the volume change during the repeated cycling processes.

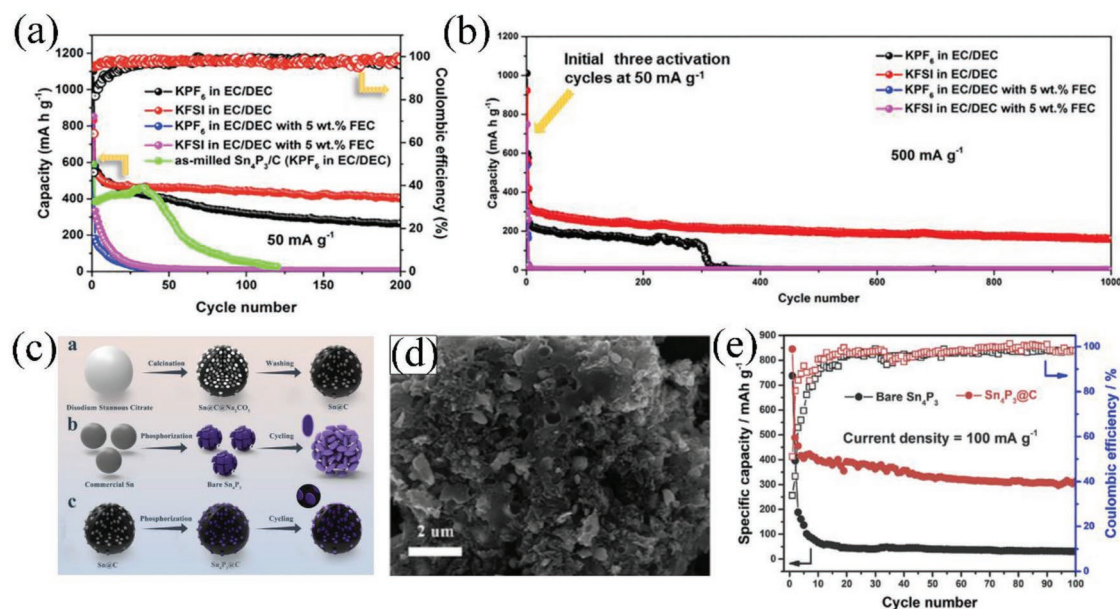


Figure 7. a,b) Cycling performance of $\text{Sn}_4\text{P}_3/\text{C}$ anode with various electrolytes at 50 and 500 mA g^{-1} , respectively. Reproduced with permission.^[24] Copyright 2018, Elsevier. c) Schematic illustration of the synthesis of Sn_4P_3 and $\text{Sn}_4\text{P}_3/\text{C}$ composite; d) SEM image of $\text{Sn}_4\text{P}_3/\text{C}$ anode; e) Cycling performance of $\text{Sn}_4\text{P}_3/\text{C}$ anode at 100 mA g^{-1} . Reproduced with permission.^[4c] Copyright 2019, Elsevier.

Table 2. Comparison of the synthetic methods, structural properties, electrolyte composition, the potassium storage mechanism and the electrochemical performance of the metal phosphides anodes in KIBs. ("x%" represents the carbon content based on the "raw material ratio").

Anode	Synthetic methods	Structural properties	Discharge products	Test methods	Electrolyte	Carbon content [wt%]	ICE	Potassium storage performance (based on the mass of composite)	Ref.
CoP ₂ /NPPCS	Self-assemble	CoP particles of tens of nanometers	—	—	1 M KPF ₆ in EC/DMC/DEC	49%	19.6%	127 mAh g ⁻¹ remained after 1000 cycles at 100 mA g ⁻¹	[47]
GeP ₃ powder	Ball-milling	Agglomerated microsized GeP ₃ particles	K ₄ P ₃ , KGe	In operando synchrotron XRD	1 M KFSI in EC/DEC	0	58.6%	495.1 mAh g ⁻¹ remained after 50 cycles at 50 mA g ⁻¹	[46]
					1 M KPF ₆ in EC/DEC		45.8%	Maintained to 220 cycles with fast capacity decay	
					1 M KFSI/ KPF ₆ +5% FEC		—	Dropped quickly at 50 mA g ⁻¹	
Sn ₄ P ₃ /C	Ball-milling	Agglomerated microsized particles	K _{3-x} P, KSn	Ex situ XRD	0.8 M KPF ₆ in EC/DEC	12.5%	—	307.2 mAh g ⁻¹ remained after 50 cycles at 50 mA g ⁻¹	[19]
Sn ₄ P ₃ @carbon fibers	Ball-milling; electrospinning	Sn ₄ P ₃ particles of about 350 nm in carbon fibers	K ₃ P, KSn	In operando synchrotron XRD	1 M KFSI in EC/DEC	40%	64.2%	403.1 mAh g ⁻¹ remained after 200 cycles at 50 mA g ⁻¹	[24]
					1 M KPF ₆ in EC/DEC		46.1%	400.8 mAh g ⁻¹ remained after 50 cycles at 50 mA g ⁻¹	
					1 M KFSI/ KPF ₆ +5% FEC		—	Dropped quickly at 50 mA g ⁻¹	
Sn ₄ P ₃ @ porous carbon	Solvothermal	Sn ₄ P ₃ particles of hundreds of nanometers in porous carbon	K _{3-x} P, KSn	Ex situ XRD; Ex situ HRTEM	0.8 M KPF ₆ in EC/DEC	—	51%	431 mAh g ⁻¹ at 100 mA g ⁻¹ with 73% after 100 cycles	[4c]

In addition, the GITT test further confirmed the mechanism behind an enhanced diffusion kinetics of the unique Sn₄P₃@C anode structure.

The synthetic methods, structural properties, electrolyte composition, the potassium storage mechanism, and electrochemical performance of the metal-phosphides anodes for KIBs are summarized in **Table 2**. According to the above-mentioned research results, the development of metal phosphide anodes for KIBs is still in its infancy. As shown in Table 2, the synthetic methods mainly focus on ball-milling that leads to the formation of simple mixture of carbon component and large irregular agglomerated metal phosphide particles with the particles size of hundreds of nanometers, which fail to achieve a full utilization of the active material and buffer the volume change during the continuous potassiation-depotassiation process. Overall, the reversible capacity and the long cycling performance are still unsatisfying. In view of the same volume effects of the metal-phosphides in KIBs with the P anode, the well integration of nanosized metal-phosphide/C composites should be further developed assisting with ball-milling, solvothermal phosphorization, and gas-solid-phase methods.

3.5. Electrolyte Optimization for Metal Phosphide Anodes

As summarized in Table 2, Zhang et al. systematically studied the influence of electrolyte composition and additives on the potassium storage performance of GeP₃ and Sn₄P₃@carbon fibers anodes.^[24,46] Obviously, the electrolyte of 1 M KFSI in

EC/DEC displays higher ICE, enhanced long cycling stability and rate capability than the electrolyte containing KPF₆ and FEC additive. Based on the study on electrochemical polarization, dendrite growth, and SEI layer composition, the authors further proposed that the KFSI potassium salt in carbonate electrolytes could effectively facilitate the uniform and thinner SEI layer formation, weaken the side reactions, suppress the growth of potassium dendrites, and reduce the effects of polarization. Meanwhile, these studies also confirmed that high fluoride concentration in the electrolyte may stimulate side reactions, leading to the poor potassium storage performance. These research results have great significance to the development of potassium ion battery system.

4. Summary and Outlook

In this progress report, recent developments of P and metal phosphide anodes for KIBs is comprehensively summarized. Although great advances have been made, some significant challenges still remain. Hence, the development of effective strategies to overcome them might accelerate the practical application of P anodes in KIBs.

- 1) Although it has been proved that P is confirmed to be a promising anode material for KIBs due to its natural abundance and the highest theoretical capacity, some undesirable issues should be solved before they can be deployed for commercial use. First of all, there is a lack of industrially

scalable production methods to synthesize P, especially those with layered structure. The existing methods present several disadvantages such as high cost, highly reactive operation processes, highly poisonous, and flammable under ambient environment. According to previous study on P anodes for KIBs, the synthetic methods of P anodes highly depend on the top-down methods by breaking down bulk red P to small particles such as ball-milling and the vaporization-condensation methods, both of which show their drawbacks. For example, the high-energy ball-milling process would destroy the morphology of the carbon matrix and result in the limited coverage with carbon component, is even not effectively to reduce the particle size of P to nanoscale level. In view of the vaporization-condensation strategy, the insufficient conversion of white P to red P during the cooling process would lead to formation of white P residues. Therefore, the exploration of effective bottom-up methods to prepare novel nanosized red P based anodes, such as the reduction of phosphorus halide precursor (PCL_3 , PCL_5 , PI_3), carbon thermal reduction of phosphorus oxide (P_4O_{10}), and hydrothermal method is highly sought after. The development of novel P nanoarchitectures combined with conductive carbon matrix, such as porous red P nanofibers and nanotubes, core-shell, yolk-shell, and some free-standing P structure provides a new platform for buffering the enormous volumetric variation of P, and thus improving the long cycling performance of KIBs. In addition, introducing heteroatoms doping into P composites to modify its electronic structure may effectively relieve the volume variation and improve the reaction activity. However, since red P precursors have only limited variety and very sensitive to water and oxygen, developing promising bottom-up method is of great significance but has a long way to go. Besides bulk red P, the use of nanosized layer-structure black P and atomically thin phosphorene as anode materials could possibly be an efficient way to buffer the volume variation problem. However, complexity of synthesis process, extremely high temperature and pressure, and low yield of black P, as well as intrinsic instability of phosphorene under oxygen-containing atmosphere substantially obstruct their broad application. Therefore, much efforts are required to develop the cost-effective and large-scale methods for preparing high quality P. Second, the stepwise alloying/dealloying process for the pure P anode still remains unknown due to different potassiation products of KP, K_4P_3 , and K_{3-x}P phases were detected in previous studies. Obviously, it is imperative to make full understanding on the mechanism on the P anode via some advanced in situ characterizations techniques. In addition, relevant theoretical calculation should be performed to theoretically describe the reaction process. By using the theoretical simulation and mathematical modeling, theoretical calculations could directly reflect the structure stability, the electrochemical reaction process, the adsorption energy and so on, which could be used to underpin the experimental results. Finally, the research of KIBs is still at a very early development stage. Hence, the exploration of P anodes that exhibit excellent structural stability, good electrical conductivity as well as outstanding potassium storage performance is the heart of all the fancy innovations in this field.

- 2) The potassium storage performance and the potassiation/depotassiation mechanism of the CoP, GeP_5 , and Sn_4P_3 anodes in recent studies have been systematically illustrated. Both of the GeP_5 and Sn_4P_3 anodes undergo the conversion-alloying mechanism, leading the formation of final potassiation products of $\text{KGe/K}_4\text{P}_3$ and $\text{KSn/K}_3\text{P}$, respectively. Although the potassiation products were all evaluated via the in operando synchrotron XRD tests, different potassiation products were detected for the P component. These results are controversial and still needed to be further evaluated. In addition, the reported GeP_5 , Sn_4P_3 , and CoP anodes for KIBs are large particles or aggregates of ten to hundreds of nanometers fabricated by the ball-milling or the self-assembly strategy, which is not beneficial for the fast charge transfer and K^+ diffusion. A better morphological control and size restriction on metal phosphides can be achieved through phosphidation and solvothermal phosphidation of relevant precursors such as metal oxides or sulfides with novel morphology. In addition, hybridization strategy to combine nanosized metal phosphides with conductive carbon matrix in a more effective way should be developed to enhance the synergistic effect between these two species. Up to now, only limited variety of metal phosphides was reported. Considering the promising results delivered by the aforementioned metal phosphides, further investigation into other viable candidates in this family, especially those P-rich metal phosphides (SnP_3 , NiP_3 , and CuP_2), represent a possible future research for KIBs.
- 3) The above-mentioned phosphorus and metal phosphide anodes in KIBs all deliver much lower ICE less than 60% with large irreversible capacity loss, which may be ascribed to the decomposition of electrolyte, the formation of SEI film as well as the irreversible insertion of K^+ on the defective sites. In a full battery, the low ICE and CE of the anode material will lead to significant consumption of the K^+ provided by the cathode, which causes a fast capacity fading. In order to improve the ICE of the phosphorus and metal phosphide anodes, the assembling of the primary P/C particles into the large-sized secondary particles could effectively increase the packing density and decrease the side reactions during charge/discharge. In addition, a protective layer on the nanosized P particles surface may be an effective strategy to modify the electrode surface chemistry and reduce the side reactions. Except for the electrode materials, other components, such as potassium salts, electrolyte additives, and binders have great influence on the electrochemical performance especially the ICE as illustrated in this progress report.
- 4) Given the rapid development of wearable electronic devices and roll-up displays, integration of flexible electrode materials with related energy storage devices has become one of the most fascinating research directions. In this regard, the fabrication of KIBs that features low-cost, flexible, and high-performance is of significance. As reported, P-based electrode materials, such as black P and phosphorene, have been practically used in flexible LIBs, which are capable of delivering high capacity, excellent rate capability, and prolonged cycling stability. Following the same trend, P-based electrode materials can also serve as the promising flexible electrode materials for low-cost flexible KIBs.

While challenges still exist to put P and metal phosphides into real practice, both of them show great potential in KIBs applications based on their intrinsic properties. Therefore, the structural design strategies, characterization methods, potassium storage mechanism, and the improvement of potassium storage capability still needs to be further investigated and could serve as a model for other kinds of alloying-based anode materials applied in energy storage systems. Design prototypes full-cell of KIBs with phosphorus-based anode materials is the next vital task. Given the recent development of P-based nanostructures and nanocomposite construction, it should not be long before we see phosphorus-based electrode materials can be incorporated in potassium-ion full batteries.

Acknowledgements

This work was supported by the National Key R&D Research Program of China (Nos. 2018YFB0905400, 2016YFA0200200, and 2016YBF0100100), the National Natural Science Foundation of China (Nos. 51622210, 51872277, 21605136, 51572259, and 51872283), the DNL cooperation Fund, CAS (DNL180310, DNL180308), the Natural Science Foundation of Liaoning Province (Grant No. 20180510038), DICP (DICP ZZBS201708, DICP ZZBS201802), DICP&QIBEBT (Grant No. DICP&QIBEBT UN201702), the LiaoNing Revitalization Talents Program (Grant XLYC1807153).

Conflict of Interest

The authors declare no conflict of interest.

Keywords

alloying-based anode, anode materials, phosphorus-based composites, potassium-ion batteries

Received: March 4, 2019

Revised: July 22, 2019

Published online:

- [1] a) L. Lu, X. Han, J. Li, J. Hua, M. Ouyang, *J. Power Sources* **2013**, 226, 272; b) N. Nitta, F. Wu, J. T. Lee, G. Yushin, *Mater. Today* **2015**, 18, 252.
- [2] J. Heyd, G. E. Scuseria, M. Ernzerhof, *J. Chem. Phys.* **2003**, 118, 8207.
- [3] a) M. D. Slater, D. Kim, E. Lee, C. S. Johnson, *Adv. Funct. Mater.* **2013**, 23, 947; b) S. W. Kim, D. H. Seo, X. Ma, G. Ceder, K. Kang, *Adv. Energy Mater.* **2012**, 2, 710; c) Z. Jian, W. Luo, X. Ji, *J. Am. Chem. Soc.* **2015**, 137, 11566; d) S. Komaba, T. Hasegawa, M. Dahbi, K. Kubota, *Electrochem. Commun.* **2015**, 60, 172.
- [4] a) Z. Jian, Z. Xing, C. Bommier, Z. Li, X. Ji, *Adv. Energy Mater.* **2016**, 6, 1501874; b) J. Zhao, X. Zou, Y. Zhu, Y. Xu, C. Wang, *Adv. Funct. Mater.* **2016**, 26, 8103; c) D. Li, Y. Zhang, Q. Sun, S. Zhang, Z. Wang, Z. Liang, P. Si, L. Ci, *Energy Storage Mater.* **2019**, <https://doi.org/10.1016/j.ens.2019.04.037>.
- [5] a) I. Sultana, M. M. Rahman, T. Ramireddy, Y. Chen, A. M. Glushenkov, *J. Mater. Chem. A* **2017**, 5, 23506; b) X. Wu, D. P. Leonard, X. Ji, *Chem. Mater.* **2017**, 29, 5031.
- [6] M. Okoshi, Y. Yamada, S. Komaba, A. Yamada, H. Nakai, *J. Electrochem. Soc.* **2017**, 164, A54.
- [7] W. Luo, J. Wan, B. Ozdemir, W. Bao, Y. Chen, J. Dai, H. Lin, Y. Xu, F. Gu, V. Barone, *Nano Lett.* **2015**, 15, 7671.
- [8] Z. Wang, S. M. Selbach, T. Grande, *RSC Adv.* **2014**, 4, 4069.
- [9] a) Z. Jian, S. Hwang, Z. Li, A. S. Hernandez, X. Wang, Z. Xing, D. Su, X. Ji, *Adv. Funct. Mater.* **2017**, 27, 1700324; b) C. Chen, Z. Wang, B. Zhang, L. Miao, J. Cai, L. Peng, Y. Huang, J. Jiang, Y. Huang, L. Zhang, *Energy Storage Mater.* **2017**, 8, 161.
- [10] a) Y. Xu, C. Zhang, M. Zhou, Q. Fu, C. Zhao, M. Wu, Y. Lei, *Nat. Commun.* **2018**, 9, 1720; b) R. Hao, H. Lan, C. Kuang, H. Wang, L. Guo, *Carbon* **2018**, 128, 224.
- [11] a) B. Kishore, G. Venkatesh, N. Munichandraiah, *J. Electrochem. Soc.* **2016**, 163, A2551; b) H. Izawa, S. Kikkawa, M. Koizumi, *J. Phys. Chem.* **1982**, 86, 5023.
- [12] X. Ren, Q. Zhao, W. D. McCulloch, Y. Wu, *Nano Res.* **2017**, 10, 1313.
- [13] Y. Dong, Z.-S. Wu, S. Zheng, X. Wang, J. Qin, S. Wang, X. Shi, X. Bao, *ACS Nano* **2017**, 11, 4792.
- [14] H. Gao, T. Zhou, Y. Zheng, Q. Zhang, Y. Liu, J. Chen, H. Liu, Z. Guo, *Adv. Funct. Mater.* **2017**, 27, 1702634.
- [15] V. Lakshmi, Y. Chen, A. A. Mikhaylov, A. G. Medvedev, I. Sultana, M. M. Rahman, O. Lev, P. V. Prihodchenko, A. M. Glushenkov, *Chem. Commun.* **2017**, 53, 8272.
- [16] a) Q. Wang, X. Zhao, C. Ni, H. Tian, J. Li, Z. Zhang, S. X. Mao, J. Wang, Y. Xu, *J. Phys. Chem. C* **2017**, 121, 12652; b) I. Sultana, T. Ramireddy, M. M. Rahman, Y. Chen, A. M. Glushenkov, *Chem. Commun.* **2016**, 52, 9279.
- [17] a) C. Han, K. Han, X. Wang, C. Wang, Q. Li, J. Meng, X. Xu, Q. He, W. Luo, L. Wu, *Nanoscale* **2018**, 10, 6820; b) Z. Yi, N. Lin, W. Zhang, W. Wang, Y. Zhu, Y. Qian, *Nanoscale* **2018**, 10, 13236; c) V. Gabaudan, R. Berthelot, L. Stievano, L. Monconduit, *J. Phys. Chem. C* **2018**, 122, 18266.
- [18] R. Zhang, J. Bao, Y. Wang, C.-F. Sun, *Chem. Sci.* **2018**, 9, 6193.
- [19] W. Zhang, J. Mao, S. Li, Z. Chen, Z. Guo, *J. Am. Chem. Soc.* **2017**, 139, 3316.
- [20] H. Kim, J. C. Kim, M. Bianchini, D. H. Seo, J. Rodriguez-Garcia, G. Ceder, *Adv. Energy Mater.* **2018**, 8, 1702384.
- [21] a) L. Wang, X. He, J. Li, W. Sun, J. Gao, J. Guo, C. Jiang, *Angew. Chem., Int. Ed.* **2012**, 51, 9034; b) W. Li, Z. Yang, M. Li, Y. Jiang, X. Wei, X. Zhong, L. Gu, Y. Yu, *Nano Lett.* **2016**, 16, 1546.
- [22] P. Xiong, P. Bai, S. Tu, M. Cheng, J. Zhang, J. Sun, Y. Xu, *Small* **2018**, 14, 1802140.
- [23] H. Liu, Y. Du, Y. Deng, D. Y. Peide, *Chem. Soc. Rev.* **2015**, 44, 2732.
- [24] W. Zhang, W. K. Pang, V. Sencadas, Z. Guo, *Joule* **2018**, 2, 1534.
- [25] J. M. Sangster, *J. Phase Equilib. Diffus.* **2010**, 31, 68.
- [26] Y. Wu, S. Hu, R. Xu, J. Wang, Z. Peng, Q. Zhang, Y. Yu, *Nano Lett.* **2019**, 19, 1351.
- [27] W.-J. Li, S.-L. Chou, J.-Z. Wang, H.-K. Liu, S.-X. Dou, *Nano Lett.* **2013**, 13, 5480.
- [28] J. Sun, H.-W. Lee, M. Pasta, Y. Sun, W. Liu, Y. Li, H. R. Lee, N. Liu, Y. Cui, *Energy Storage Mater.* **2016**, 4, 130.
- [29] a) C. Liu, X. Han, Y. Cao, S. Zhang, Y. Zhang, J. Sun, *Energy Storage Mater.* **2019**, 20, 343; b) F. Yang, H. Gao, J. Chen, Z. Guo, *Small Methods* **2017**, 1, 1700216; c) D. Zhao, L. Zhang, C. Fu, J. Zhang, C. Niu, *Nano Res.* **2019**, 12, 1.
- [30] W. C. Chang, J. H. Wu, K. T. Chen, H. Y. Tuan, *Adv. Sci.* **2019**, 6, 1801354.
- [31] a) W.-J. Li, S.-L. Chou, J.-Z. Wang, H.-K. Liu, S.-X. Dou, *J. Mater. Chem. A* **2016**, 4, 505; b) J. Sun, G. Zheng, H.-W. Lee, N. Liu, H. Wang, H. Yao, W. Yang, Y. Cui, *Nano Lett.* **2014**, 14, 4573; c) J. Song, Z. Yu, M. L. Gordin, S. Hu, R. Yi, D. Tang, T. Walter, M. Regula, D. Choi, X. Li, *Nano Lett.* **2014**, 14, 6329; d) S. Yao, J. Cui, J. Huang, J. Q. Huang, W. G. Chong, L. Qin, Y. W. Mai, J. K. Kim, *Adv. Energy Mater.* **2018**, 8, 1702267.
- [32] X. Wu, W. Zhao, H. Wang, X. Qi, Z. Xing, Q. Zhuang, Z. Ju, *J. Power Sources* **2018**, 378, 460.

- [33] D. Liu, X. Huang, D. Qu, D. Zheng, G. Wang, J. Harris, J. Si, T. Ding, J. Chen, D. Qu, *Nano Energy* **2018**, 52, 1.
- [34] H. Gao, T. Zhou, Y. Zheng, Y. Liu, J. Chen, H. Liu, Z. Guo, *Adv. Energy Mater.* **2016**, 6, 1601037.
- [35] J. Zhou, X. Liu, W. Cai, Y. Zhu, J. Liang, K. Zhang, Y. Lan, Z. Jiang, G. Wang, Y. Qian, *Adv. Mater.* **2017**, 29, 1700214.
- [36] S. Liu, H. Xu, X. Bian, J. Feng, J. Liu, Y. Yang, C. Yuan, Y. An, R. Fan, L. Ci, *ACS Nano* **2018**, 12, 7380.
- [37] S. Liu, H. Xu, X. Bian, J. Feng, J. Liu, Y. Yang, C. Yuan, Y. An, R. Fan, L. Ci, *J. Mater. Chem. A* **2018**, 6, 12992.
- [38] J. Qian, X. Wu, Y. Cao, X. Ai, H. Yang, *Angew. Chem., Int. Ed.* **2013**, 52, 4633.
- [39] W.-C. Chang, J.-H. Wu, K.-T. Chen, H.-Y. Tuan, *Adv. Sci.* **2019**, 6, 1801354.
- [40] a) Y. Kim, Y. Kim, A. Choi, S. Woo, D. Mok, N. S. Choi, Y. S. Jung, J. H. Ryu, S. M. Oh, K. T. Lee, *Adv. Mater.* **2014**, 26, 4139; b) W.-J. Li, Q.-R. Yang, S.-L. Chou, J.-Z. Wang, H.-K. Liu, *J. Power Sources* **2015**, 294, 627; c) W.-J. Li, S.-L. Chou, J.-Z. Wang, H.-K. Liu, S.-X. Dou, *Chem. Commun.* **2015**, 51, 3682.
- [41] a) Y. Lu, P. Zhou, K. Lei, Q. Zhao, Z. Tao, J. Chen, *Adv. Energy Mater.* **2017**, 7, 1601973; b) W. Li, S. L. Chou, J. Z. Wang, J. H. Kim, H. K. Liu, S. X. Dou, *Adv. Mater.* **2014**, 26, 4037; c) X. Fan, J. Mao, Y. Zhu, C. Luo, L. Suo, T. Gao, F. Han, S. C. Liou, C. Wang, *Adv. Energy Mater.* **2015**, 5, 1500174.
- [42] W. Zhang, M. Dahbi, S. Amagasa, Y. Yamada, S. Komaba, *Electrochem. Commun.* **2016**, 69, 11.
- [43] Z. Liu, S. Yang, B. Sun, X. Chang, J. Zheng, X. Li, *Angew. Chem., Int. Ed.* **2018**, 130, 10344.
- [44] J. Fullenwarth, A. Darwiche, A. Soares, B. Donnadieu, L. Monconduit, *J. Mater. Chem. A* **2014**, 2, 2050.
- [45] W. Li, L. Ke, Y. Wei, S. Guo, L. Gan, H. Li, T. Zhai, H. Zhou, *J. Mater. Chem. A* **2017**, 5, 4413.
- [46] W. Zhang, Z. Wu, J. Zhang, G. Liu, N.-H. Yang, R.-S. Liu, W. K. Pang, W. Li, Z. Guo, *Nano Energy* **2018**, 53, 967.
- [47] J. Bai, B. Xi, H. Mao, Y. Lin, X. Ma, J. Feng, S. Xiong, *Adv. Mater.* **2018**, 30, 1802310.
- [48] Y. Wei, J. Chen, J. He, R. Qin, Z. Zheng, T. Zhai, H. Li, *ACS Appl. Mater. Interfaces* **2018**, 10, 32162.